INVESTIGATION OF THE EFFECT OF DIFFERENT THICKNESSES AND THERMAL ANNEALING ON THE OPTICAL PROPERTIES OF $GaAs_{0.1}P_{0.89}N_{0.01}$ ALLOYS GROWN ON GaP SUBSTRATES

H. A. Alburaih [1,2], H. Albalawi [1,2] and M. Henini [2]

[1]Physics Department, Faculty of Science, Princess Nourah Bint Abdulrahman University, Riyadh, Saudi Arabia
[2]School of physics and Astronomy, University of Nottingham, Nottingham NG7 2RD, United Kingdom

ABSTRACT

This work investigates the effect of the thickness of the epitaxial layer (100nm and 1μm) on the optical properties of quaternary $GaAs_{0.1}P_{0.89}N_{0.01}$ alloys. Furthermore, the effect of rapid thermal annealing (RTA) on their properties has been studied using the Photoluminescence (PL) technique. Increasing the thickness of the epilayer led to an enhancement of the PL intensity as well as the energy bandgap, which was shifted to higher energy (from 1.82 eV in 100nm to 1.94 eV in 1μm layer). However, the 1.94 eV bandgap energy is not ideal for solar cells based materials grown on GaP substrates. Post-growth thermal annealing by rapid thermal annealing (RTA) for both samples resulted in an enhancement in the optical properties as observed by a decrease of the Full Width at Half Maximum (FWHM) and an increase of the PL intensity. Therefore, all results obtained in this study indicate that $GaAs_{0.1}P_{0.89}N_{0.01}$ with 100nm epilayer thick is better choice to fabricate good efficiency solar cells based materials on GaP substrates as compared to 1μm sample.

KEY WORDS: Photoluminescence, Molecular Beam Epitaxy, Dilute Nitrides, GaAsPN, Rapid Thermal Annealing (RTA)

INTRODUCTION

Utilization of light-converting materials has been considered as an attractive strategy to improve light harvesting abilities. One of this class of materials is dilute III-V nitride alloys which have recently attracted a great deal of attention for applications in optoelectronics particularly for solar cells [1-2]. Among these alloys, GaAsPN is an interesting material for pseudomorphic integration of photonics with silicon [3-4]. This material also can be adjusted to the desired wavelengths required for several applications, for example achieving 1.8 eV bandgap material lattice matched to Si for solar cell devices, which is the main aim of its use in this work.

One of the most effective parameters in the growth of dilute nitrides is the thickness of the epilayer [5]. The thickness has been reported to influence the lattice matching of the materials as well as the structural, optical and electrical properties [6]. Moreover, it is very important to keep the thickness of the epilayer in the range of the critical thickness (CT) (1 μm within the CT range of GaAsPN alloy).

It is worth pointing out that the efficiency of solar cells is affected by different parameters such as the electronic quality of the top and bottom materials of solar cells, the bandgap and the thickness [5].

This work investigates the effect of the thickness on the optical properties of $GaAs_{0.1}P_{0.89}N_{0.01}$ epilayer (100nm and 1μm) grown by Molecular Beam Epitaxy (MBE) on (100) GaP substrates using PL technique. Furthermore, the PL technique is performed also to study the effect of RTA on the optical properties of both $GaAs_{0.1}P_{0.89}N_{0.01}$ samples.

EXPERIMENTAL DETAILS

In this letter, GaAsPN quaternary structures are grown in a solid source MBE system on GaP(100) substrates, which uses a valved RF plasma source to incorporate nitrogen into GaP lattice. These were capped with 10nm GaP layers. The growth temperature was 480 °C. These samples were grown under a low V/III flux with a Beam Equivalent Pressure (BEP) ratio of 10. The phosphorus flux was 5 μTorr. The nominal nitrogen composition for the samples investigated is 1%.

Temperature dependent photoluminescence (PL) experiment, which is a very powerful optical characterisation technique, has been used in this study to assess the optical quality of the as-grown and annealed used semiconductor structures.

The wavelength and the pumping power density were equal to 405nm and 15mW/cm^2, respectively. Samples were mounted in a helium-closed cycle cryostat to study PL from 10K to 300K. In particular, significant parameters such as PL intensity, bandgap energy and full width at half maximum (FWHM) can be determined using PL.

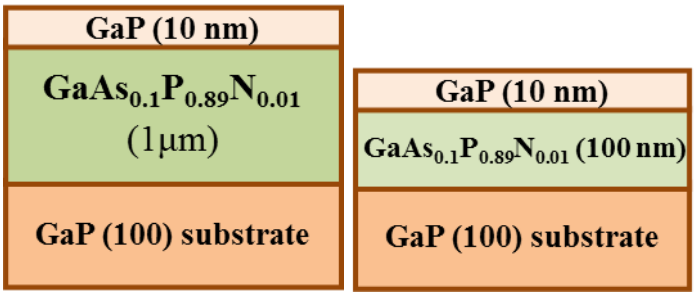

Figure 1: Schematic diagram of GaAsPN dilute nitride with two epilayer thicknesses **(a)** 1μm **(b)** 100 nm and with similar nitrogen nominal composition of 1%.

RESULTS AND DISCUSSION

A. THICKNESS – DEPENDENT PHOTOLUMINESCENCE

To study the effect of thickness on the optical quality of $GaAs_{0.1}P_{0.89}N_{0.01}$ epilayer grown on GaP (100) substrates, PL measurements were performed at 10 K on two $GaAs_{0.1}P_{0.89}N_{0.01}$ epilayers with thicknesses of 100 nm and 1μm as shown in Fig. 2.

Some small differences have been observed in their PL properties. An intense PL signal is observed for both samples indicating an effective optical emission. However, the 100 nm and 1μm samples have different PL emission energies at 1.82eV and 1.94eV, respectively. This could be due to an enhanced incorporation of As and N in the 100 nm GaAsPN sample leading to a much more reduced band gap of GaP than the 1μm GaAsPN sample.

.

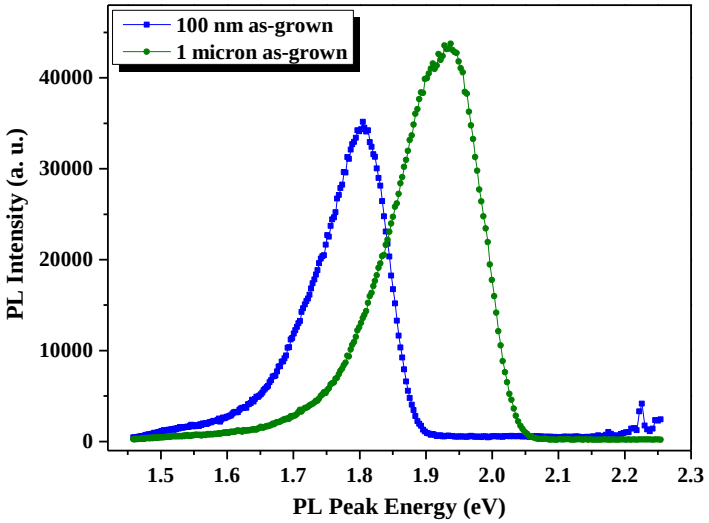

Figure 2: PL peak intensity vs photon energy of 1μm and 100nm $GaAs_{0.1}P_{0.89}N_{0.01}$ at 10 K.

It is clear that $GaAs_{0.1}P_{0.89}N_{0.01}$ material with thicker epitaxial layer shows a higher luminescence intensity at 10 K than the thinner epilayer (~ 1.3 times higher).

However, the PL spectra for both samples are broad. This broadening could be related to the effects of radiative recombination via localized states within the band gap due to structural disorder [7]. Nevertheless, the 1 μm sample exhibits higher PL intensity due most probably to the smaller contribution of the above effects [7]. In addition, as shown in Figure 3 the quenching temperature of the PL signal for the 1 μm sample (~300K) is higher than that of the 100 nm sample (~200K). These results suggest that the 1 μm sample should exhibit better electrical properties due to its higher PL intensity and higher quenching temperature as will be discussed in the following sections. In addition, our findings also support the argument that the larger contribution of the above effects with low PL intensity and low quenching temperature in the thinner sample might be strain related due to the high lattice mismatch [9]. Therefore, one should expect that optimized growth parameters for the fabrication of thin samples will avoid phase separation in order to enhance the electrical properties of the dilute nitride alloys [10].

Fig. 3 shows the temperature dependence of the PL peak energy and FWHM of 1 μm and 100 nm $GaAs_{0.1}P_{0.89}N_{0.01}$ epilayers. For both samples, the shift of the temperature has an opposite behaviour to the shift of the band gap. From Fig. 3 it can be seen that the bandgap energy of the thicker sample is higher than the thinner one throughout the temperature range 10 K- 300 K.

Previous optical modelling studies demonstrated strong relation between lattice mismatch and thickness of the film [11]. Depending on the top layer's band gap and quantum efficiency, the thickness should yield a current – matched tandem structure at a current level that changes only with the top layer of the cell. It is well-known that higher conversion efficiencies can be achieved by reducing the film thickness [5,12].

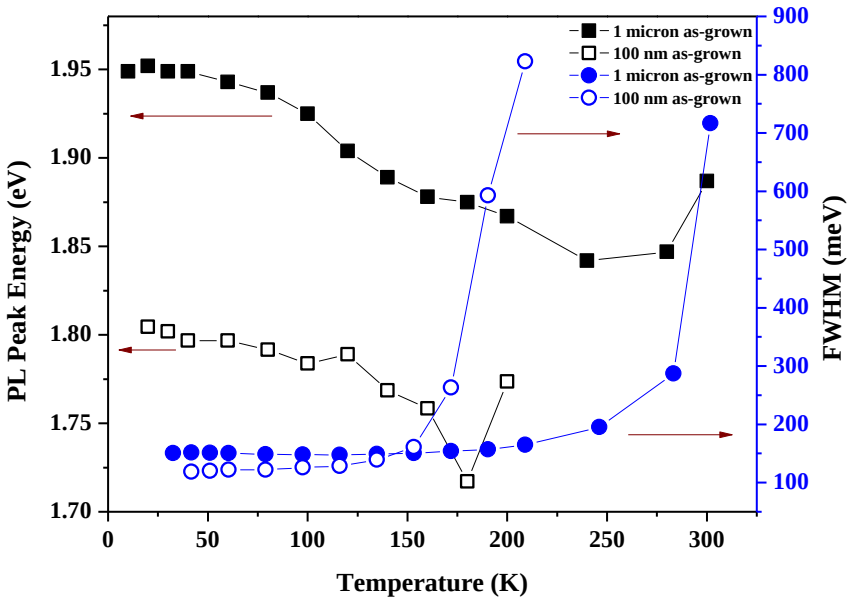

Figure 3: Temperature dependence of the PL peak energy and FWHM for 1 μm and 100 nm $GaAs_{0.1}P_{0.89}N_{0.01}$ epilayers.

The temperature dependence of the PL spectra has been used to investigate the behaviour of defects which were explained using the strong electron-phonon coupling which is described in terms of configuration coordinate (CC) model [13] where the electronic states interact with the localized vibration modes. With increasing temperature, the higher phonon states of the excited states are occupied and the full width half maximum (FWHM) increases according to CC-model [14].

In order to investigate the temperature dependence of PL intensities and explain nonradiative recombination process for 100 nm and 1 μm $GaAs_{0.1}P_{0.89}N_{0.01}$ epilayers, the temperature dependent integrated PL intensity is plotted in Figure 4 as a function of reciprocal temperature. The behaviour is characterized by two different temperature ranges, corresponding to two thermally activated nonradiative recombination processes. The fits are derived by applying the formalism described in [15] and are performed using equation.

$$I(T) = \left[\frac{I_0}{1 + \alpha_1 e^{\frac{-E_{a1}}{kT}} + \alpha_2 e^{\frac{-E_{a2}}{kT}}} \right] \qquad (1)$$

where I(T)and I_0 is the integrated PL intensity at TK and 0K, respectively. α_1 and α_2 are constants related to the density of nonradiative centers, E_{a1} and E_{a2} are thermal activation energies of these centers. , and *k* is the Boltzmann constant.

It is important to point out that it is difficult to determine all the parameters precisely that as there are many fitting parameters in Equation 1. Therefore, in order to make the fitting process relevant, an understanding of the possible physical origin of the two activation processes in the samples investigated is required. In this work, we believe that nitrogen is the main origin of the nonradiative recombination defects in our $GaAs_{0.1}P_{0.89}N_{0.01}$ samples.

Fig. 4 shows the integrated PL intensity versus 1/T of 100 nm and 1 μm $GaAs_{0.1}P_{0.89}N_{0.01}$ epilayers and the Arrhenius fitting. As can be seen in Fig. 4, at low temperatures for both samples, the integrated PL intensity does not change appreciably with temperature. However, at high temperatures, it decreased more rapidly with temperature [16]. This behaviour suggests that two nonradiative recombination processes occur, corresponding to two different activation energies at these two temperature ranges. As shown in Figure 3, the quenching temperature of the PL signal for the 1 μm sample (~300K) is higher than that of the 100 nm sample (~200K). These results further confirm that the the 1 μm sample has lower nonradiative defect density, and therefore high optical quality of the active region [7]. Table 1 presents the values of E_{a1} and α_1 (corresponding to the low-temperature range)

and E_{a2} and α_2 (corresponding to the high-temperature range) for 100 nm and 1 µm $GaAs_{0.1}P_{0.89}N_{0.01}$ samples. The nonradiative recombination at low temperature is typically due to the capture process of excitons by defects. The smaller thermal activation energy means that thermally activated nonradiative recombination can easily occur in thinner samples than thicker samples. This means that the PL signal of thinner samples vanishes at much lower temperatures than the thicker samples as clearly shown in Figure 4. The decrease of E_{a1} observed in thinner samples can be explained by enhanced incorporation of N as demonstrated by a red shift shown in Figure 2. At high temperature, the nonradiative recombination process with activation energy E_{a2} governs. For the thinner sample, we obtained activation energy value of E_{a1}= 17.2. This value is lower than that of the thicker sample, which can be attributed to carriers at localized states because of different N clusters or alloy disorder caused by N incorporation fluctuation. It can clearly be seen in Table 1 that α_1, which is related to the density of nonradiative centres, increases from 7 to 21 as the epilayer decreases from 1 µm to 100 nm in agreement with the conclusion that the nitrogen incorporation in the thinner epilayer is higher than that of the thicker one, and N is the main origin of nonradiative defects in our samples.

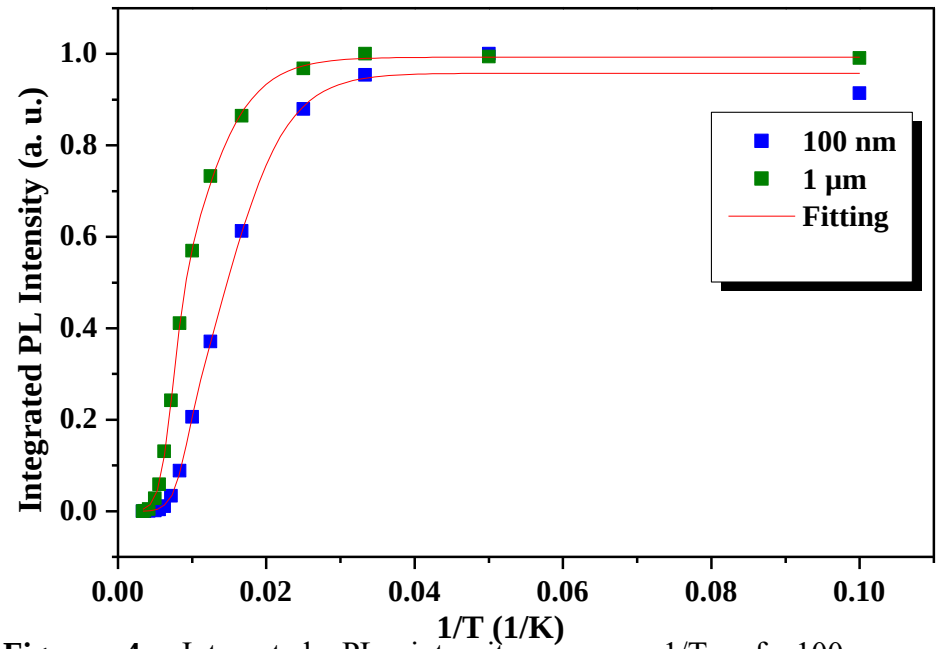

Figure 4: Integrated PL intensity versus 1/T of 100 nm and 1 µm $GaAs_{0.1}P_{0.89}N_{0.01}$epilayers and Arrhenius fitting.

Table 1 shows clearly that the values of the two activation energies increase with increasing the epilayer thickness. The activation energies and α constants of the 100 nm $GaAs_{0.1}P_{0.89}N_{0.01}$ sample are found to be equal to 17.2 meV and 65.8 meV, and 21 and 7641, respectively. The activation energies and α constants values of the 1μm sample are 20.5 meV and 110 meV, and 7 and 16070, respectively.

Table 1: Arrhenius's parameters obtained from the integrated PL peak intensity versus 1/T results for as-grown 100 nm and 1 μm $GaAs_{0.1}P_{0.89}N_{0.01}$epilayers grown on GaP substrates.

Thickness	**E_{a1} (meV)**	**E_{a2} (meV)**	**α_1**	**α_2**
100 nm	17.2	65.8	21	7641
1 μm	20.5	110	7	16070

Thus, all the above results show that increasing the thickness of the epilayer of dilute $GaAs_{0.1}P_{0.89}N_{0.01}$ material from 100 nm to 1 μm leads to an enhancement of the PL intensities and activation energy, except the FWHM in the temperature range 10 - 140K. In addition, the bandgap shifts towards higher energy (from 1.82 eV to ≃1.94 eV) with increasing the thickness from 100 nm to 1 μm. Therefore, for solar cell applications, $GaAs_{0.1}P_{0.89}N_{0.01}$ based devices need to fullfil two major requirements: (i) the epilayer should be thin so that one can achieve the optimum bandgap energy for optimum absorption (~1.82 eV), and (ii) the relatively larger density of non-radiative centres (electrically active centres) observed in thin samples should be reduced in order to improve the electrical quality of the devices. Although thick $GaAs_{0.1}P_{0.89}N_{0.01}$ epilayers exhibit higher PL intensities than thin layers, their energy gap at ~1.94 eV is less suitable for solar cells based materials grown on Si substrates.

B. RAPID THERMAL ANNEALING –DEPENDENT PHOTOLUMINESCENCE

Figures 5 and 6 present the photon energy with luminescence intensity for the 100 nm and 1 μm thick $GaAs_{0.1}P_{0.89}N_{0.01}$ alloys before and after RTA, respectively. It can be seen that the annealing process leads to an enhancement of the optical properties as demonstrated by the PL intensity increase by approximately a factor of 13 in 100 nm and 2.4 in 1 μm at 10 K, respectively.

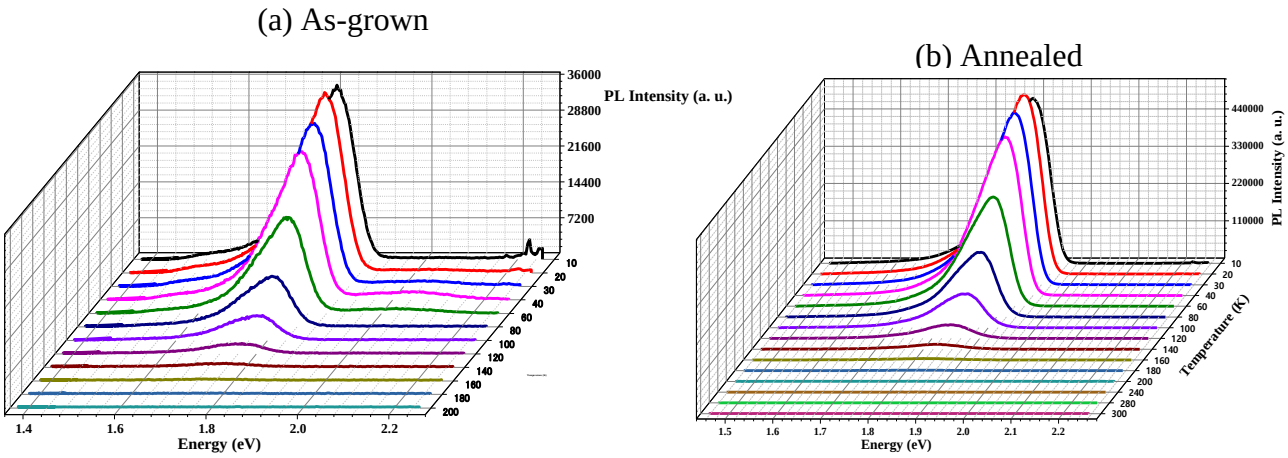

Figure 5: PL intensity vs photon energy at different temperatures for (a) as-grown and (b) annealed of $GaAs_{0.1}P_{0.89}N_{0.01}$ with epilayer thickness of 100 nm. Note that the two y-axis values of the as-grown and annealed samples are different.

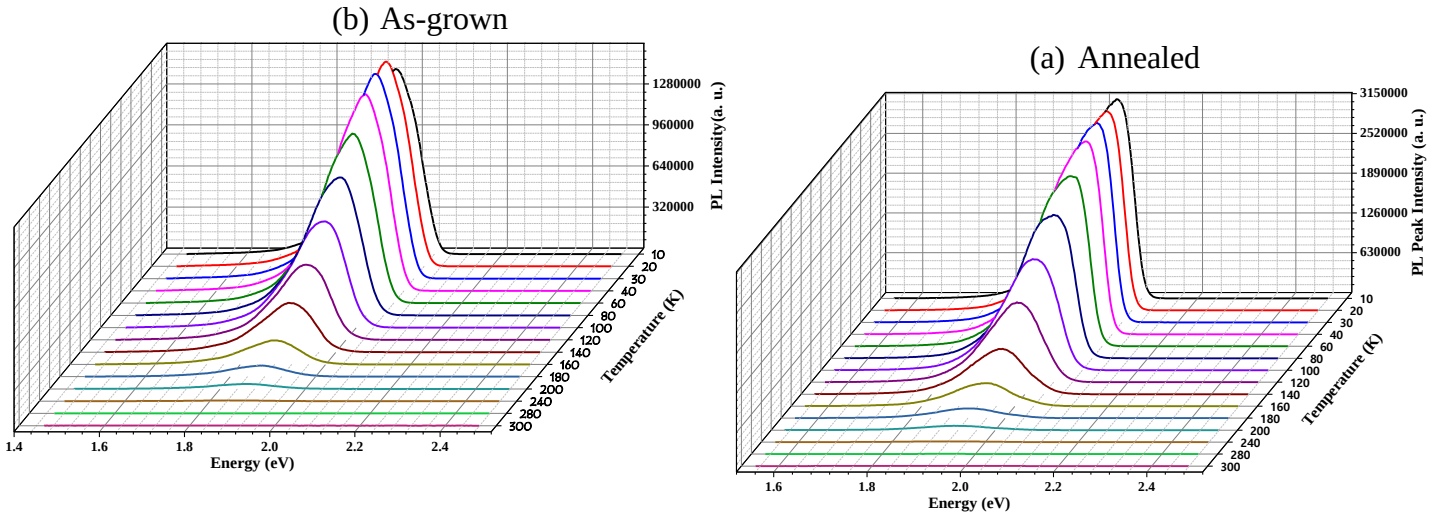

Figure 6: PL intensity vs photon energy from 10 K to 300 K (a) as-grown and (b) annealed of $GaAs_{0.1}P_{0.89}N_{0.01}$ with epilayer thickness of 1 μm. Note that the two y-axis values of the as-grown and annealed samples are different.

This is not a surprise in dilute nitride materials, as the N incorporation into GaAsP leads to the presence of a random distribution of nitrogen clusters and isolated

nitrogen impurity states in the crystals [17-18]. By subjecting this alloy to an RTA temperature of 800°C, a thermal energy applied for the change in group V atom configuration i.e., a change in the nearest neighbour environment of Ga atoms [19]. This significantly results in a reduction in the defect density and an increase in layer absorption [19-20]. In addition, after RTA a blue-shift is observed at all temperatures. This is clearly seen in Fig. 7, which presents the normalized PL peaks with photon energy at 10 K for 100 nm layer and Fig. 8 which illustrates the PL spectra for thicker layer at 10 K.

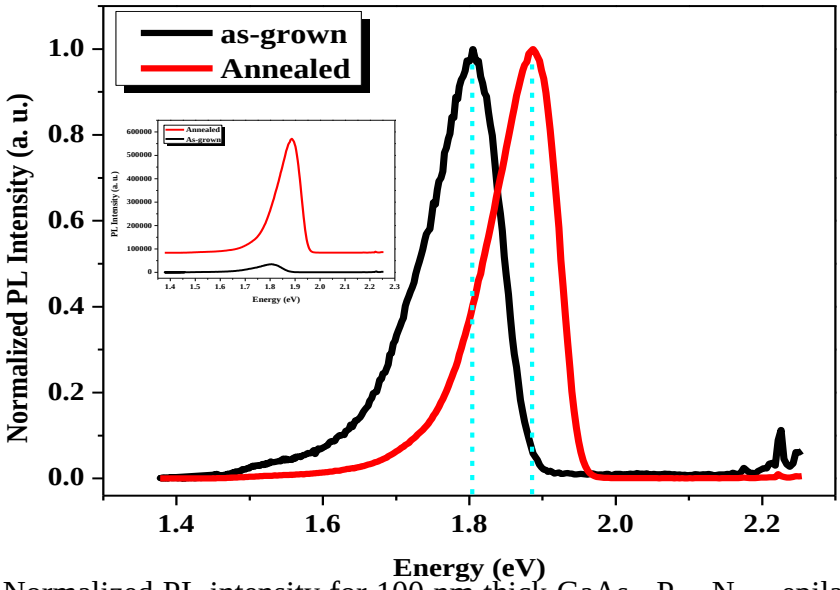

Figure 7: Normalized PL intensity for 100 nm thick $GaAs_{0.1}P_{0.89}N_{0.01}$ epilayer before and after RTA. Inset: non normalized PL intensity for $GaAs_{0.1}P_{0.89}N_{0.01}$ before and after RTA.

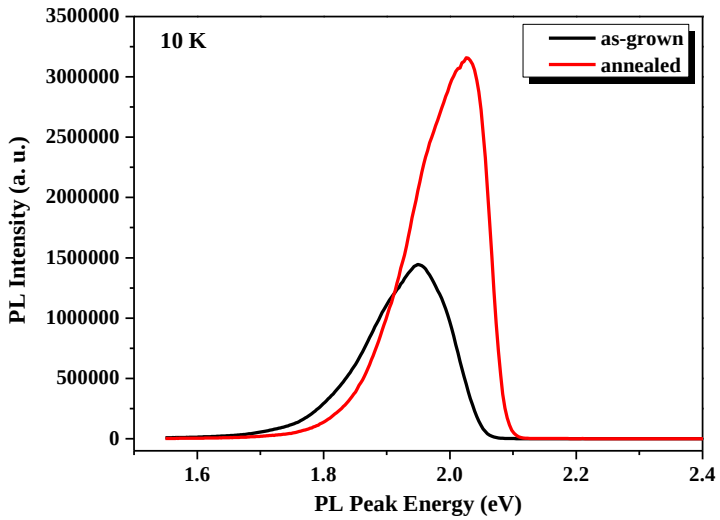

Figure 8: PL spectra at 10 K of 1µm thick $GaAs_{0.1}P_{0.89}N_{0.01}$ epilayer before and after RTA.

Obviously, in Fig 7 the PL energy shifts to higher energy (from 1.8 eV to ≃ 1.9 eV) after annealing treatment. In addition, in Fig 8 the energy of the 1µm of $GaAs_{0.1}P_{0.89}N_{0.01}$ shifts also to a higher value after annealing (from 1.95 eV to 2.1 eV). The mechanism of this could be attributed to the fact that by annealing the increase in the luminescence intensity evidences a decrease of point defects in the layers and /or radiative localised states in the bandgap [21-22]. Moreover, this shift could be attributed to the fact that annealing can yield [23].

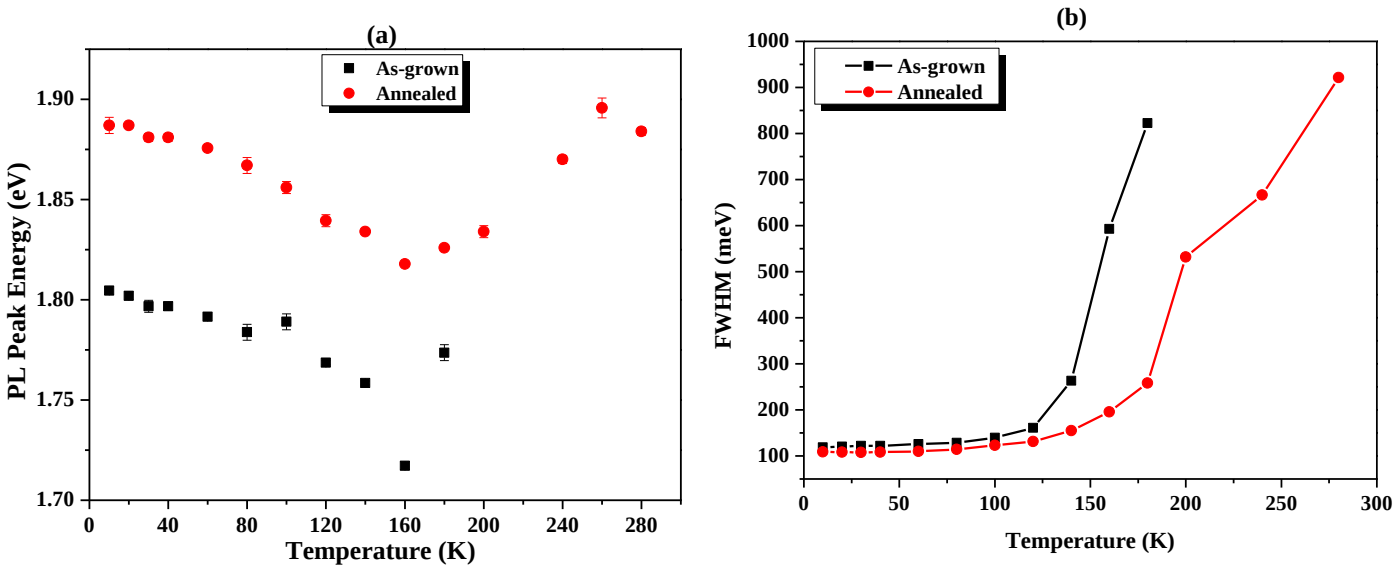

Figure 9: (a) Temperature dependence of PL peak energy and (b) FWHM of 100 nm $GaAs_{0.1}P_{0.89}N_{0.01}$ alloys before and after RTA.

In III-V-N dilute nitrides it is very significant to plot the temperature dependence of the PL peak energy before and after RTA in order to study the effect of localization on the bandgap. The PL peak energy positions and FWHM of the as-grown and annealed of 100 nm and 1µm thick $GaAs_{0.1}P_{0.89}N_{0.01}$ alloys over the temperature range 10-300K are plotted in Fig. 9 and Fig. 10 , respectively. From Fig. 10 (a) it is observed that the 1µm thick as-grown $GaAs_{0.1}P_{0.89}N_{0.01}$ sample has a bandgap energy showing an S-shape (up-down-up) over the temperature range 10K- 300K. This means that this sample has been affected by the localized states phenomenon, which is reported for a number of dilute nitrides materials. This phenomenon mainly happens due to the nitrogen incorporation and its effect on the conduction band of the materials [24], which confirms that N incorporation has a strong effect on this sample

since RTA annealing has not led to a reduction or elimination of the S-shape as it is reported for other III-V-N dilute nitride semiconductors [25].

It is worth pointing out that 100 nm as-grown sample does not display clearly the well-known S-shape. However, the S-shape behaviour is also observed in the annealed samples (see Fig. 9 (a)). This impact could be explained by the fact that the incorporation of N atoms into the host lattice results in the reduction (compensation) of strain introduced by the incorporation of high As content in GaAsPN. Additionally, as in (Ga,In)(N,As) epilayers [26], the chemical bonding properties at the surface during the growth of GaAsPN with high As composition play an important role and could favour Ga-N bonds. This would result in an enhancement of the N incorporation into the host lattice.

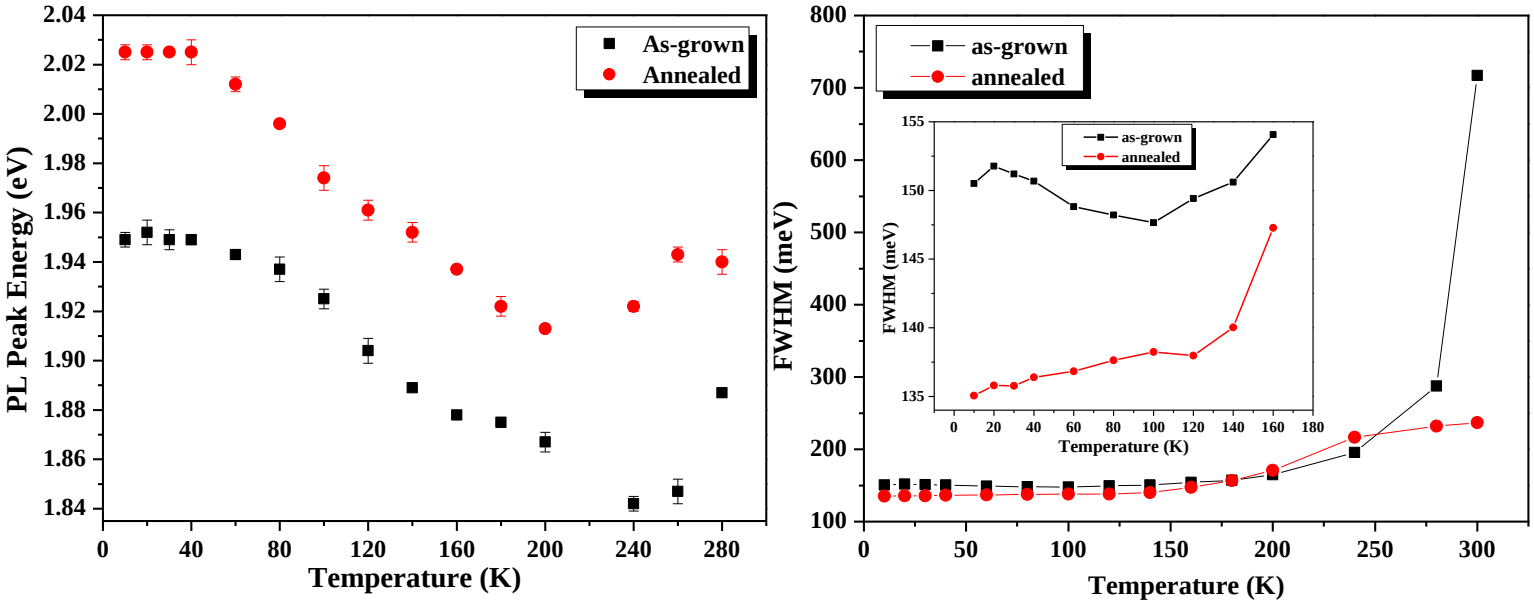

Figure 10: (a) Temperature dependence of PL peak energy and (b) FWHM of 1 µm $GaAs_{0.1}P_{0.89}N_{0.01}$ alloys before and after RTA. Inset: FWHM of 1µm $GaAs_{0.1}P_{0.89}N_{0.01}$ alloys before and after RTA in the temperature range 10 K – 160 K.

In Fig. 10 (b), the FWHM results show a strong dependence on the annealing. After RTA, the FWHM decreases to almost a value of 150 meV from approximately 300

meV at 140 K as the inset in Fig 10 (b) shows. Furthermore, it can be noted from Fig. 10 (b) that the RTA treatment improved significantly the FWHM by narrowing its values throughout the temperature range 10 K-300 K. This reduction in the FWHM is indicative of a reduction of the point and radiative defects after RTA, which indicates the enhancement of $GaAs_{0.1}P_{0.89}N_{0.01}$ layer quality after RTA.

For a further understanding of the RTA effect on the optical properties, the PL integrated intensities as a function of temperature for as-grown and annealed $GaAs_{0.1}P_{0.89}N_{0.01}$ with thick 100 nm and 1 μm are plotted in Fig. 11 and 12, respectively. In addition, the Arrhenius equation is used to fit these data to calculate the activation energy (E) and the corresponding constant α related to the density of nonradiative centers. It is very obvious from Fig. 11 and 12 that the integrated PL intensity decreases as the temperature is increased in both as-grown and annealed samples. Also, it is very clear from the inset in Fig. 11 and 12 that the RTA treatment leads to an enhancement of the integrated PL intensity. This is could be related to the fact that thermal annealing treatment of $GaAs_{0.1}P_{0.89}N_{0.01}$ alloy reduces the non-radiative defects such as As_{Ga} antisites and Ga_i self- interstitials [27].

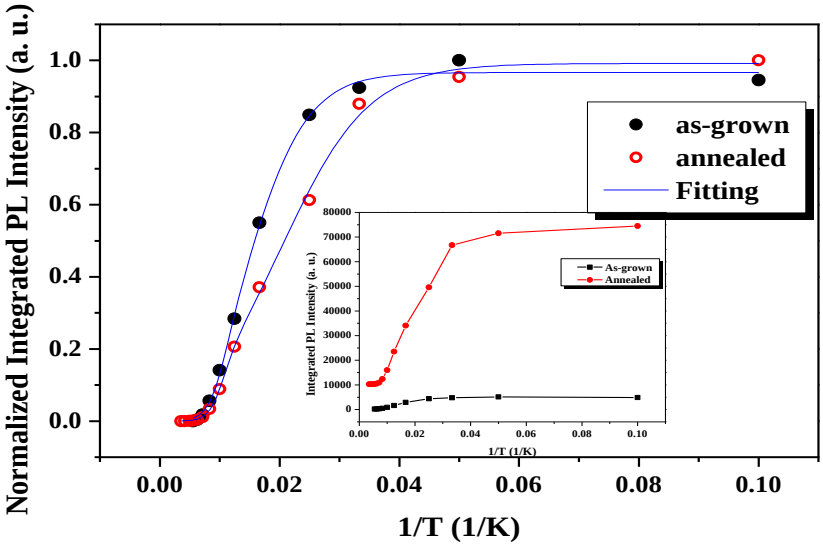

Figure 11: Temperature dependence of the integrated PL intensity of 100 nm thick $GaAs_{0.1}P_{0.89}N_{0.01}$ alloys before and after RTA, with Arrhenius fitting (blue lines). Inset: Non normalized integrated PL intensity for $GaAs_{0.1}P_{0.89}N_{0.01}$ alloys before and after RTA.

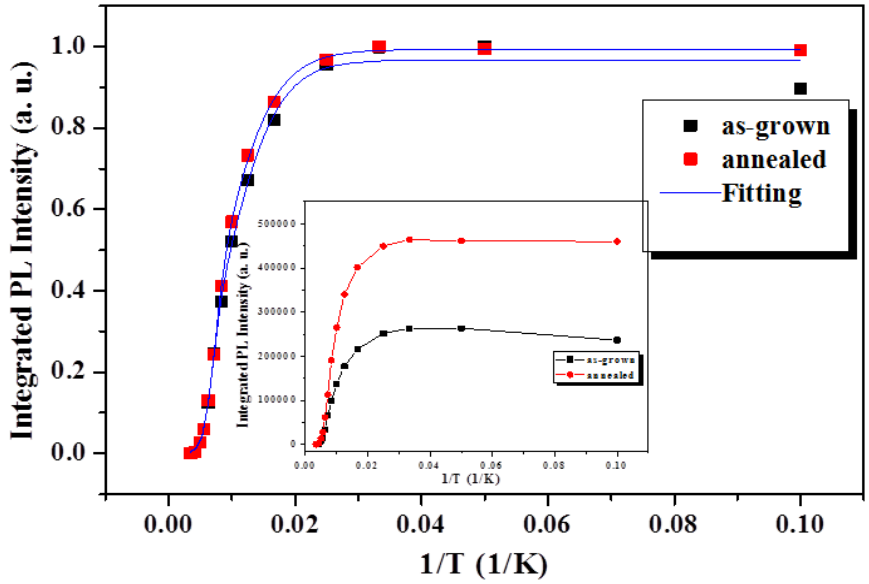

Figure 12: Integrated PL intensity versus 1/T before and after RTA annealing of 1 µm thick $GaAs_{0.1}P_{0.89}N_{0.01}$epilayers. Inset: Non normalized Integrated PL intensity of 1 µm $GaAs_{0.1}P_{0.89}N_{0.01}$epilayers before and after RTA.

Table 2 and 3 displays the values of thermal activation energies as well as the corresponding constants α related to the density of nonradiative for 100 nm and 1 µm thick, respectively. The presence of two quenching processes indicates that there are at least two types of non-radiative defects in the sample. For the 100 nm thick as-grown $GaAs_{0.1}P_{0.89}N_{0.01}$ alloys, the thermal activation energies E_{a1} and E_{a2}, and corresponding constants α_1 and α_2 are 17.2 and 65.8 meV, and 21 and 7641, respectively. These values increased after annealing treatment. After RTA, the thermal activation energies E_{a1} and E_{a2} are found to be 21.1 and 78.5 meV, respectively, and the corresponding ratios α_1, α_2 are also increased by increasing the activation energy to be 28.5 and 51949 after RTA.

Table 2: Arrhenius's parameters for the integrated PL peak intensity for as-grown and annealed 100 nm thick $GaAs_{0.1}P_{0.89}N_{0.01}$ epilayer grown on GaP substrates.

Sample	E_{a1} meV	E_{a2} meV	α_1	α_2
as-grown $GaAs_{0.1}P_{0.9}N_{0.01}$	17.2	65.8	21	7641
annealed $GaAs_{0.1}P_{0.9}N_{0.01}$	21.1	78.5	28.5	51949

Table 3: Arrhenius's parameters obtained from the integrated PL peak intensity versus 1/T results for as-grown and annealed 1μm $GaAs_{0.1}P_{0.89}N_{0.01}$ epilayers grown on GaP substrate.

Sample	E_{a1} meV	E_{a2} meV	α_1	α_2
as-grown $GaAs_{0.1}P_{0.9}N_{0.01}$	20.5	110	7	16070
annealed $GaAs_{0.1}P_{0.9}N_{0.01}$	21.5	124.5	10	39795

The activation energies E_{a1} and E_{a2} for as-grown and annealed 1 μm thick $GaAs_{0.1}P_{0.89}N_{0.01}$ alloy are found to be 20.5 eV and 110 eV, and 21.5 eV and 124.5 eV, respectively. This indicates that annealing leads to an enhancement of the activation energies, which could be due to a reduction of N related defects that are not known up to the present [21]. Moreover, the α constants also increased by RTA from 7 and 16070 to 10 and 39795, respectively, as shown in Table 3. Additional structural studies need to be carried out in order to identify which defects correspond to these activation energies and also to measure the concentration of these defects.

It is important to point out the that the α values increase while the PL intensities increase for both samples after annealing, which is contradictory. However, as explained in the previous sections these are fitting parameters obtained from a simple

model and one has to be cautious not to draw conclusions based only on the α values. Our explanation is based as follows: for the annealed samples the integrated PL intensity increases, however, the PL peak blue shifts meaning that there could be less nitrogen incorporation or a rearrangement of N environment in our samples as explained above. This is also reflected in the higher values of E_{a1} after annealing for both samples.

It is worth comparing the activation energies of the annealed $GaAs_{0.1}P_{0.89}N_{0.01}$ samples having 100 nm and 1μm thickness. As can be seen in Table 4, the thicker layer has higher values of the activation energies E_{a1} (21.5 eV) and E_{a2} (124.5 eV) as compared to the thinner sample (E_{a1} = 21.1 eV and E_{a2} = 78.5 eV). This could be assigned to the reported fact that the thicker layer has large non-radiative centres density than the thinner one.

The α constants decrease from 28.5 and 51949 for annealed 100nm thickn sample to 10 and 39795 for annealed 1 μm thickn sample, respectively. This unexpected behaviour of reduced α values of the thicker sample after RTA is at present unclear.

Table 4: Arrhenius's parameters obtained from the integrated PL peak intensity versus 1/T results for annealed 100nm and 1 μm $GaAs_{0.1}P_{0.89}N_{0.01}$epilayers grown on GaP substrates.

Sample	**Thickness**	**E_{a1} meV**	**E_{a2} meV**	**α_1**	**α_2**
annealed $GaAs_{0.1}P_{0.9}N_{0.01}$	100nm	21.1	78.5	28.5	51949
annealed $GaAs_{0.1}P_{0.9}N_{0.01}$	1μm	21.5	124.5	10	39795

CONCLUSION

Photoluminescence (PL) measurements were performed to investigate the effect of the thickness of the epitaxial layer (100nm and 1μm) on the optical properties of quaternary $GaAs_{0.1}P_{0.89}N_{0.01}$ alloys. Furthermore, PL was used to study the effect of rapid thermal annealing on their optical properties.

It was observed that increasing the epilayer thickness leads to an enhancement of the PL intensity as well as the energy bandgap which was shifted to higher energy (from 1.82 eV in 100nm to 1.94 eV in 1μm layer). The bandgap energy of 1.94 eV is not ideal for solar cells based materials grown on GaP substrates. Due to the large thickness, the effect of strain on bandgap is pronounced and is accompanied by a large lattice mismatch. The enhancement in the PL intensity and bandgap energy was explained by the fact that the thicker layer has larger free exciton radiative recombination centres with low defect densities. However, the100nm thick quaternary $GaAs_{0.1}P_{0.89}N_{0.01}$ alloy has a bandgap energy which is best suited for solar cell devices grown on Si substrates. The lower optical quality of the thinner samples may be due to more clustering of N and carrier localization at N pairs and clusters.

After RTA the PL peak intensities of both samples with different thicknesses increased, at the same time the bandgap energies shifted to higher values. In $GaAs_{0.1}P_{0.89}N_{0.01}$ alloy after RTA the blue-shift was attributed to the rearrangement of N environment in such quaternary materials. An S-shape was observed for both as-grown and annealed 1 μm thick $GaAs_{0.1}P_{0.89}N_{0.01}$ samples. This is due to the effect of localization, which is caused by N incorporation in $GaAs_{0.1}P_{0.89}N_{0.01}$ semiconductors. Furthermore, narrower FWHM from 10K to 300K and larger activation energies were obtained after RTA due to a reduction in the density of defects.

ACKNOWLEDGMENTS

This research project was granted by the deanship of scientific research in Princess Nourah bint Abdulrahman University, Riyadh, KSA.

Moreover, we would like to acknowledge C. Cornet, S. Almosni and Y. Léger at the University of Rennes, INSA Rennes, CNRS, Institute FOTON, France, for the growth of the samples, which have been studied in this paper.

REFERENCES:

[1] S. Almosni, P. Rale, C. Cornet, M. Perrin, L. Lombez , A. Létoublon, K. Tavernier , C. Levallois, T. Rohel, N. Bertru, J. Guillemoles, and O. Durand. Solar Energy Materials and Solar Cells. Elsevier, **147**, pp.53 (2016).

[2] M. Wiemer, V. Sabnis, and H. Yuen, Proc. SPIE **8108**, 810804 (2011).

[3] K. Kharel, and A. Freundlich, Appl. Phys. Lett. **124**, 095104 (2018).

[4] S. Almosni, C. Robert, T. Nguyen Thanh, C. Cornet, A. Létoublon, T. Quinci, C. Levallois, M. Perrin, J. Kuyyalil, L. Pedesseau, A. Balocchi, P. Barate, J. Even, J. Jancu, N. Bertru, X. Marie, O. Durand, and A. Le Corre, Appl. Phys. Lett. **113**, 123509 (2013).

[5] J. Olson, S. Kurtz, A. Kibbler, and P. Faine, Appl. Phys. Lett. **56**, 623 (1990).

[6] S. Kurtz, P. Faine, and J. Olson, Appl. Phys. Lett. **68**, 1890 (1990).

[7] Mark. Fox, optical properties of solid, 2nd edition, oxford press (2010).

[8] X.Tixir, M.Adamcy, T.Tiedje, S.Francoeur, A.Mascarenhas, P.Wei and F.Schiettekatte, Appl.Phys.Lett.82 (14) 2245 (2003)

[9] S.Almosni, C. Robert, T. Nguyen, C. Cornet, A. Létoublon. J.App.Phys. **113**, 123509 (2013).

[10] I. Buyanova, W. Chen, Physics and Applications of Dilute Nitrides, Taylor & Francis Books, Inc., New York, (2004).

[11] J.M.Olson, S.R.Kurtz, A.E.Kibber and P.Faine, Appl.Phus, Lett,56 623(1990)

[12] A. Cornet, T. Nguyen , T. Quinci, S. Almosni, T. Rohel, J. Kuyyalil, A. Rambaud, A. Létoublon, N. Bertru, O. Durand, and A. LeCorre, Appl. Phys. Lett. **101**, 251906 (2012).

[13] S. Shinoya, T.Koda, K Era and HFujiwara, J.Phy.Soc.Jpn19, 1157(1964)

[14] M.A.Reshchikov and H.Morkoc. Journal of applied physics,97, 061301(2005)

[15] H. Sun, S. Calvez, M. Dawson, J. Gupta, G. Aers, and G. Sproule, Appl. Phys. Lett. **89**, 101909 (2006).

[16] M. Muhammed, N.Alwadai, S.Lopatin, A.Kuramata and I.Roqan, Applied Materials and Interfaces, 9 (39), 34057 (2017)

[17] H. Saito, T. Makimoto, T. Nishida, and N. Kobayashi, Appl. Phys. Lett. **70**, 2984 (1997).

[18] K. Volz, J. Koch, B. Kunert, I. Nemeth, and W. Stolz, Jornal of Crystal Growth **298**, pp. 126, (2007).

[19] S.Francoeur, S. Nikishin, C. Jin, Y. Qiu, and H. Temkin, Appl. Phys. Lett. **75**, 1538 (1999)

[20] O. Rubel, M. Galluppi, S. Baranovskii, K. Volz, L. Geelhaar, H. Riechert, P. Thomas, and W. Stolz, Appl. Phys. Lett. **98**, 063518 (2005).

[21] B. Kunert, D. Trusheim, V. Voßebürger, K. Volz, and W. Stolz, Physica Status Solidi (A) **205**, pp. 114 (2008).

[22] C. Cornet, T. Nguyen Thanh, T. Quinci, S. Almosni, T. Rohel, J. Kuyyalil, A. Rambaud, A. Létoublon, N. Bertru, O. Durand, and A. Le Corre, Appl. Phys. Lett. **101**, 251906 (2012).

[23] P. Klar, H. Grünning, J. Koch, S. Schäfer, K. Volz, W. Stolz, W. Heimbrodt, A. Saadi, A. Lindsay, and E. O'Reilly, Phys. Rev. B **64**, 121203 (2001).

[24] S. Mazzucato, R. Potter, A. Erol, N. Balkan, P. Chalker, T. Joyce, T. Bullough, X. Marie, H. Carrère, E. Bedel, G. Lacoste, A. Arnoult, and C. Fontaine, Phys. E Low-Dimens. Syst. Nanostructures **17**, 242 (2003).

[25] W. Chen, I. Buyanova, C. Tu, and H. Yonezu. Acta Physica Polonica, Vol. **108** (2005).

[26] R. Kudrawiec, M. Latkowska, M. Baranowski, J. Misiewicz, L. Li, and J. Harmand, Phys. Rev. B **88**, 125201 (2013).